



Reduced global warming from CMIP6 projections when weighting models by performance and independence

Lukas Brunner¹, Angeline G. Pendergrass^{2,1}, Flavio Lehner¹, Anna L. Merrifield¹, Ruth Lorenz¹, and Reto Knutti¹

¹Institute for Atmospheric and Climate Science, ETH Zurich, Universitätsstrasse 16, 8092 Zurich, Switzerland

²National Center for Atmospheric Research, Boulder, Colorado, US

Correspondence: Lukas Brunner (lukas.brunner@env.ethz.ch)

Abstract. The sixth Coupled Model Intercomparison Project (CMIP6) constitutes the latest update on expected future climate change based on a new generation of climate models. To extract reliable estimates of future warming and related uncertainties from these models, the spread in their projections is often translated into probabilistic estimates such as mean and likely range. Here, we use a model weighting approach, which accounts for a model's historical performance based on several diagnostics as well as possible model inter-dependence within the CMIP6 ensemble, to calculate constrained distributions of global mean temperature change. We investigate the skill of our approach in a perfect model test, where we remove each CMIP6 model from the ensemble in turn, use it as pseudo-observation in the historical period, and evaluate the weighted CMIP6 ensemble against it in the future. This is complemented by a second perfect model test drawing on the previous-generation CMIP5 models as pseudo-observations. In addition, we show that our independence diagnostics correctly clusters models known to be similar based on a CMIP6 “family tree”, which enables applying a weighting based on the degree of inter-model dependence. We then apply the weighting approach, based on two observational estimates (ERA5 and MERRA2), to constrain CMIP6 projections in weak (SSP1-2.6) and strong (SSP5-8.5) climate change scenarios. Our results show a reduction in projected mean warming for both scenarios because some CMIP6 models with high future warming receive systematically lower performance weights. The mean of end-of-century warming (2081-2100 relative to 1995-2014) for SSP5-8.5 with weighting is 3.7 °C, compared to 4.1 °C without weighting; the likely (66 %) uncertainty range is 3.1 °C to 4.6 °C, a decrease of 13 %. For SSP1-2.6, weighted end-of-century warming is 1 °C (0.7 °C to 1.4 °C). Applying the weighting to estimates of Transient Climate Response (TCR) yields 1.9 °C (1.6 °C to 2.1 °C – a reduction in the likely uncertainty range of 46 %), which is consistent with estimates from previous model generations and other lines of evidence.

1 Introduction

Projections of future climate by Earth System Models provide a crucial source of information for adaptation planning, mitigation decisions, and the scientific community alike. Many of these climate model projections are coordinated and provided within the frame of the Coupled Model Intercomparison Projects (CMIPs), which are now in phase 6 (Eyring et al., 2016). A typical way of communicating information from such multi-model ensembles (MMEs) is by combining them into probabilistic distributions,



25 such as a best estimate and uncertainty range. In doing so it is important to make sure that the different sources of uncertainty
are identified, discussed, and accounted for, to provide reliable information without being overconfident. Typically three main
sources of uncertainty are identified in MMEs: (i) uncertainty in future emissions, (ii) internal variability of the climate system,
and (iii) model response uncertainty (e.g., Hawkins and Sutton, 2009; Knutti et al., 2010).

30 Uncertainty due to future emissions can easily be isolated by making projections conditional on scenarios such as the Shared
Socioeconomic Pathways (SSPs) in CMIP6 (O'Neill et al., 2014) or the Representative Concentration Pathways (RCPs) in
CMIP5 (van Vuuren et al., 2011). The other two sources of uncertainty are harder to quantify since reliably separating them is
often challenging (e.g., Kay et al., 2015; Maher et al., 2019). Model uncertainty arises due to different responses and feedbacks
of models to a given radiative forcing, leading to different estimates of mean warming or Transient Climate Response (TCR)
(e.g., Forster et al., 2013). Such different responses to the same forcing can emerge, among other things, due to different
processes and feedbacks as well as due to the parametrisations used in the different models (e.g., Zelinka et al., 2020). Internal
35 variability stems from the chaotic behavior of the climate system and is highly dependent on the variable of interest as well
as the period and region averaged over. While, for example, uncertainty in global mean temperature is mainly dominated by
differences between models, regional temperature trends are considerably more dependent on internal variability as can be
estimated from Single Model Initial-condition Large Ensembles (SMILEs) (Lehner et al., 2020; Maher et al., 2019; Merrifield
et al., 2019).

40 Depending on the composition of the investigated MME, uncertainty estimates often fail to reflect that included models are
not always independent from each other. In the development process of climate models, ideas, code and even full components
are shared between institutions or models might be branched from each other in order to investigate specific questions. This can
lead to some models (or model components) being copied more often, resulting in an over-representation of their respective
internal variability or sensitivity to forcing (Bishop and Abramowitz, 2013; Boé, 2018; Boé and Terray, 2015). The CMIP
45 MMEs in particular have not been designed with the aim of including only independent models and are therefore sometimes
referred to as “ensembles of opportunity” (e.g., Tebaldi and Knutti, 2007) incorporating as many models as possible. When
calculating probabilities based on such MMEs it is therefore important to account for model inter-dependence in order to
accurately translate model spread into estimates of mean change and related uncertainties.

50 In addition, not all models represent the aspects of the climate system relevant to a given question equally well. To account
for that, a variety of different approaches have been used to weight, sub-select, or constrain models based on their historical
performance. This has been done both regionally and globally as well as for a range of different target metrics such as end-of-
century temperature change or TCR (see, e.g., Brunner et al., 2020b; Eyring et al., 2019; Knutti et al., 2017a, for an overview).
Global mean temperature increase in particular is one of the most widely discussed effects of continuing climate change and the
main focus of many public and political discussions. With the release of the new generation of CMIP6 models, this discussion
55 has been sparked yet again, as several CMIP6 models show stronger warming than most of the earlier-generation CMIP5
models (Forster et al., 2020; Zelinka et al., 2020; Swart et al., 2019; Gettelman et al., 2019; Voldoire et al., 2019; Golaz et al.,
2019; Andrews et al., 2019). This raises the question of whether these models are accurate representations of the climate system



and what that means for the interpretation of the historical climate record and the expected change due to future anthropogenic emissions.

60 Here, we use the Climate model Weighting by Independence and Performance (ClimWIP) method (e.g., Merrifield et al., 2019; Brunner et al., 2019; Knutti et al., 2017b) to weight models in the CMIP6 MME. Weights are based on (i) each models performance in simulating historical properties of the climate system such as horizontally resolved anomaly, variability, and trend fields, and (ii) its independence from the other models in the ensemble, estimated based on shared biases of climatology. In contrast to many other methods, which constrain model projections based on only one observable quantity, such as the warming trend (e.g., Giorgi and Mearns, 2002; Ribes et al., 2017; Jiménez-de-la Cuesta and Mauritsen, 2019; Nijssen et al., 2020; Tokarska et al., 2020), ClimWIP is based on multiple diagnostics, representing different aspects of the climate system. These diagnostics are chosen to evaluate a model's performance in simulating observed climatology, variability, and trend patterns. Note that, in contrast to other approaches such as emergent constraint-based methods, some of these diagnostics might not be highly correlated with the target metric (however, it is still important that they are physically relevant – to avoid introducing noise without useful information in the weighting). Combining a range of relevant diagnostics is less prone to overconfidence, since the risk of up-weighting a model because it “accidentally” fits observations for one diagnostic, while being far away from them in several others is greatly reduced. In turn, methods which are based on such a basket of diagnostics have been found to generally lead to weaker constraints (Sanderson et al., 2017; Brunner et al., 2020b), as the effect of the weighting typically weakens when adding more diagnostics (Lorenz et al., 2018).

75 ClimWIP has already been used to create estimates of regional change and related uncertainties for a range of different variables such as Arctic sea ice (Knutti et al., 2017b), Antarctic ozone concentrations (Amos et al., 2020), North American maximum temperature (Lorenz et al., 2018) and European temperature and precipitation (Merrifield et al., 2019; Brunner et al., 2019). Here, we focus on investigating the ClimWIP methods performance in weighting global mean temperature changes when informed by different diagnostics. To assess the robustness of these choices, we perform an out-of-sample perfect model test using CMIP5 and CMIP6 as pseudo-observations. Based on these results, we select a combination of diagnostics which capture not only a model's transient warming but also its ability to reproduce historical patterns in climatology and variability fields in order to increase the robustness of the weighting scheme and minimize the risk of skill decreases due to the weighting. This approach is particularly important for users interested in the “worst case” rather than in mean changes. We also look into the inter-dependencies among the models, showing the ability of our diagnostics in clustering models with known shared components using a “family tree” (Masson and Knutti, 2011; Knutti et al., 2013) and further the skill of the independence weighting to account for this. We then calculate combined performance-independence weights based on two reanalysis products in order to also account for the uncertainty in the observational record. Finally, we apply these weights to provide constrained distributions of future warming and CTR.



2 Data and Methods

90 2.1 Model data

The analysis is based on all currently available CMIP6 models which provide surface air temperature (tas) and sea level pressure (psl) for the historical, SSP1-2.6, and SSP5-8.5 experiments. We use all available ensemble members, which is a total of 129 runs from 33 models (see table S3 in the supplementary material for a full list including references). We use models post-processed within the ETH Zurich CMIP6 next generation archive, which provides additional quality checks and re-grids models onto a common $2.5^\circ \times 2.5^\circ$ latitude-longitude grid, using second order conservative remapping (see Brunner et al., 2020a, for details). In addition, we use the first member of all CMIP5 models providing the same variables and the corresponding experiments (historical, RCP2.6, RCP8.5) which is a total of 27 models (see table S4 for a full list).

2.2 Reanalysis data

To represent historical observations in tas and psl we use two reanalysis products: ERA5 (C3S, 2017) and MERRA2 (Gelaro et al., 2017; GMAO, 2015a, b). Both products are regridded to a $2.5^\circ \times 2.5^\circ$ latitude-longitude grid using second order conservative remapping and are evaluated in the period 1980-2014. Within the framework of the model weighting, they are combined to provide an estimate of observational uncertainty (see Brunner et al., 2019, for details). Finally, we also compare our results to globally averaged merged temperatures from the Berkley Earth Surface Temperature (BEST) data set.

2.3 Model weighting scheme

105 We use an updated version of the ClimWIP method described in Merrifield et al. (2019) and Brunner et al. (2019), which is based on earlier work by Lorenz et al. (2018), Knutti et al. (2017b), Sanderson et al. (2015b), and Sanderson et al. (2015a); it can be downloaded at: <https://github.com/lukasbrunner/ClimWIP.git>. It assigns a weight w_i to each model m_i that accounts for both model performance as well as independence,

$$w_i = \frac{e^{-\left(\frac{D_i}{\sigma_D}\right)^2}}{1 + \sum_{j \neq i}^M e^{-\left(\frac{S_{ij}}{\sigma_S}\right)^2}}, \quad (1)$$

110 where D_i and S_{ij} are the generalised distances of model m_i to the observations and to model m_j , respectively. The shape parameters σ_D and σ_S set the strength of the weighting, effectively determining the point at which a model is considered to be “close” to the observations or to another model (c.f., section 2.5).

This updated version of ClimWIP assigns the same weight to each initial-condition ensemble member of a model, which is adjusted by the number of ensemble members (see the revised version of Merrifield et al., 2019, for a detailed discussion).

115 To illustrate this additional step in the weighting method, consider a single performance diagnostic d . d is calculated for each model and ensemble member separately, hence $d = d_i^k$ with i representing individual models, and k running over all ensemble members K_i of model m_i (in CMIP6, from one to 50). For each model m_i , the mean diagnostic d_i' is,



$$d'_i = \frac{\sum_k^K d_i^k}{K_i}, \quad \text{for all } i. \quad (2)$$

d'_i is then used to calculate the generalised distance D_i and further the performance weight w_i via (1). An analogous process is used for distances between models. This setup allows a consistent comparison of model fields to each other and to observations in the presence of internal variability and, in particular, also enables the use of variance-based diagnostics. In addition, it ensures a consistent estimate of the performance shape parameter σ_D in the perfect model test (see section 2.5), based on the average weight per model; in previous work, in contrast, it was based on only one ensemble member per model.

2.4 Weighting target and diagnostics

We apply the weighting to projections of annual mean, global mean temperature change from two SSPs, representing weak (SSP1-2.6) and strong (SSP5-8.5) climate change scenarios. Changes in two 20-year target periods representing mid-century (2041-2060) and end-of-century (2081-2100) conditions are compared to a 1995-2014 baseline. In addition, we weight TCR values from all available models obtained from an update of the data set described in Tokarska et al. (2020). The weights are calculated from global, horizontally-resolved diagnostics based on annual mean data in the 35-year period 1980-2014. We use different diagnostics for the calculation of the independence and performance parts of the weighting, as proposed in the revised version of Merrifield et al. (2019).

The goal of the independence weighting is to identify structural similarities between models (such as shared offsets or similar spatial patterns) which are interpreted to be indications of inter-dependence arising from, e.g., shared components or parametrisations. In the past, combinations of horizontally-resolved regional temperature, precipitation, and sea level pressure fields, have typically been used (e.g., Brunner et al., 2019; Sanderson et al., 2017; Knutti et al., 2013; Boé, 2018; Lorenz et al., 2018). Following the work of Merrifield et al. (2019), we use a combination of two global, climatology-based diagnostics, the spatial pattern of climatological temperature (tasCLIM) and sea level pressure (pslCLIM), that were found to work well for clustering CMIP5-generation models known to be similar. This definition of independence does not hold in a purely statistical sense (Annan and Hargreaves, 2017), but we still stress that it is important to account for different degrees of model inter-dependencies as well as possible when developing probabilistic estimates from an “ensemble of opportunity” such as CMIP6. We validate this approach in section 4.2 of the results.

The performance weighting, in turn, allocates more weight to models which better represent the observed behavior of the climate system as measured by the diagnostics, while down-weighting models with large discrepancies from the observations. We use multiple diagnostics to limit overconfidence in the case where a model fits the observations well in one diagnostic by chance, while being far away from them in several others. For example, we want to avoid giving heavy weight to a model based solely on its representation of the temperature trend if its year-to-year variability differs strongly from observed year-to-year variability. The performance weights are based on five global, horizontally-resolved diagnostics: temperature anomaly (tasANOM; calculated from tasCLIM by removing the global mean), temperature variability (tasSTD), pslANOM, and pslSTD as well as temperature trend (tasTREND). We use anomalies instead of climatologies in the performance weight in order to



150 avoid punishing models for absolute bias in global-mean temperature and pressure, because these are not correlated with projected warming (Flato et al., 2013; Giorgi and Coppola, 2010). This can be different for regional cases, where, e.g., absolute temperature biases have been shown to be important for constraining projections of Arctic sea ice extent (Knutti et al., 2017b) or European summer temperatures (Selten et al., 2020).

One aim of our study is to find an optimal combination of diagnostics that successfully constrains projections for our target quantity (global temperature change) while avoiding overconfidence or susceptibility to uncertainty from internal variability. For example, tasTREND is a powerful diagnostic because of its clear physical relationship to and high correlation with projected warming (e.g., Tokarska et al., 2020; Nijse et al., 2020). However, while it has the highest correlation to the target of all investigated diagnostics, it also has the largest uncertainty due to internal variability (i.e., spread of tasTREND across ensemble members of the same model). Ideally, a performance weight is reflective of underlying model properties and does not depend on which ensemble member is chosen to represent that model (i.e., on internal variability). tasTREND does not fulfil this requirement: the spread within one model is the same order of magnitude as the spread among different models. To find a compromise, we divide our diagnostics into two groups: trend-based diagnostics (tasTREND) and not-trend based diagnostics (tasANOM, tasSTD, pslANOM, and pslSTD). Different combinations of these two groups (ranging from only not-trend based to only tasTREND) are evaluated in section 3.1 and the best performing combination is selected for the remainder of the study.

165 2.5 Calculation of the shape parameters

The shape parameters σ_D and σ_S determine the width of the Gaussian weighting functions. In case of the performance weighting, small values of σ_D lead to very aggressive weighting with a few models receiving all the weight, while large values lead to more equal weighting. To estimate a performance shape parameter σ_D that weights models based on their historical performance without being overconfident, we use the perfect model test detailed in Knutti et al. (2017b). In short, the test selects the smallest σ_D value (hence the strongest weighting) for which 80 % of perfect models fall within the 10-90 percentile range of the weighted distribution. Note that methods that simply maximize correlation of the weighted mean to the target in a perfect model test often tend to pick small values of σ_D that result in projections that are overconfident in the sense that the uncertainty ranges are too small (Knutti et al., 2017b).

The independence weighting has a subtle but fundamentally different dependence on its shape parameter σ_S : small values lead to equal weighting, as all models are considered to be independent, but so do large values, as all models are considered to be dependent. Hence, the effect of the independence weighting is strongest if the shape parameter is chosen such that it identifies clusters of models as similar (down-weighting them) while still correctly identifying models which are far from each other as independent (hence giving them relatively more weight) (see revised version of Merrifield et al., 2019, for a more detailed discussion including SMILEs). To estimate σ_S , we use the information from models with more than one ensemble member. We know that ensemble members are copies of the same model that differ only due to internal variability, and therefore we have a priori information about the correct independence weighting. σ_S is based only on historical information, and is therefore independent from the selected target period or scenario. Following the method described in detail in Brunner et al. (2019), we arrive at a value of $\sigma_S = 0.54$, which we use throughout the manuscript.



2.6 Validation of the performance weighting

185 To investigate the skill of ClimWIP in weighting CMIP6 global mean temperature change and the effect of the different diagnostic combinations (different relative importance of tasTREND) we apply a perfect model test. As a skill measure we use the continuous ranked probability skill score (CRPSS), a measure for ensemble forecast quality, defined as the relative error between the distribution of weighted models and a reference (Hersbach, 2000). Here, we define the CRPSS as relative change between the unweighted and weighted cases (in %), with positive values indicating a skill increase. The CRPSS is calculated
190 separately for both SSPs and future time periods, since we expect to find different skill for different projected climate states.

The first perfect model test is based only on the CMIP6 MME and focuses on evaluating the performance weighting (results are presented in section 3.1). We explain its implementation based on an example perfect model m_j with only one ensemble member for simplicity here: (i) the model m_j is taken as pseudo-observation and removed from the CMIP6 MME; (ii) the output from m_j during the historical period (1980-2014) is used to calculate the performance diagnostics for the remaining
195 models ($d'_{i \neq j}$); (iii) the generalised model-“observation” distances ($D_{i \neq j}$) and the performance weights ($w_{i \neq j}$) are calculated and applied to the MME (excluding m_j); (iv) the CRPSS is calculated using the future projections of m_j as reference. This is done iteratively, using each model in CMIP6 MME in turn as pseudo-observation. For perfect models with more than one ensemble member (m_j^b), all members are removed from the ensemble in (i), $d'_{i \neq j}$ is calculated for each member separately in (ii) and then averaged, and the CRPSS is also calculated for each ensemble member in (iv) and averaged.

200 We note that a similar perfect model test is also an integral part of ClimWIP as it is used to estimate the performance shape parameter σ_D (described in section 2.5), which introduces a small amount of circularity in this test. However, it is still valuable to investigate the skill of the weighting method using this test to (i) show the potential for an increase in skill through weighting, as well as the risk of a decrease, (ii) cross-check the σ_D calculation, and (iii) compare different fractions of trend-versus not-trend-based diagnostics, in order to establish the most skilful combination.

205 The second perfect model test (section 3.2) is conceptually equivalent, but pseudo-observations are drawn from CMIP5. This test has the advantages that we can always use the full CMIP6 MME (without having to remove any models) and that the perfect models have not been used to estimate σ_D and can be considered independent, at least in a methodological sense. Note that they are not necessarily independent in a model sense as several CMIP6 models descend from CMIP5 models and might be structurally similar to their predecessors, which was the case for the CMIP5 and 3 generations (Knutti et al., 2013). However,
210 there are also considerable differences between CMIP5 and 6 that arise from many years of additional model development, a longer observational record to tune to, and differing spatial resolutions. In addition, the emission scenarios that force CMIP5 and 6 (RCPs and SSPs, respectively) result in slightly different radiative forcings (Forster et al., 2020); determining how these scenario families differ is currently an active area of research. We do not discuss these similarities and differences in detail here; instead we use CMIP5 simply as a source of additional pseudo-observations to evaluate the skill of ClimWIP for weighting the
215 CMIP6 MME to improve the fit to a given CMIP5 model.



2.7 Validation of the independence weighting

To validate that the information in the diagnostics chosen for the independence weighting (tasCLIM and pslCLIM) can identify models known to be similar, we use a hierarchical clustering approach based on Müllner (2011) and implemented in the Python SciPy package (www.scipy.org). We use the linkage function with the average method applied to the horizontally-resolved distance fields between each pair of models. This approach is conceptually similar to the work from Masson and Knutti (2011) and Knutti et al. (2013) and follows their example of showing similarity as model “family trees”. The hierarchical clustering is *not* used in the model weighting itself; we use it here only to show that qualitative information about model similarity can be inferred from model output using the two chosen diagnostics and to compare it to the results from the independence weighting.

The independence weighting (denominator in equation (1)) quantifies the similarity information extracted from the pairwise distance fields via the independence shape parameter (σ_S ; see section 2.5). The independence weighting estimates where two models fall on the spectrum from completely independent to completely redundant and weights them accordingly. In order to test this approach, we successively add artificial “new” models into the CMIP6 MME: for an example model with two members (m_j^1 and m_j^2), we remove the first member and add it as additional model (m_{M+1}). In an idealized case, where all models are perfectly independent from each other and all ensemble members of a model are identical, we would expect the weight of the member that remains (m_j^2) to go down by a factor 1/2, while the weight of all other models would stay the same. However, in a real MME, where there is internal variability and complex model inter-dependencies exist, we would not necessarily expect such simple behaviour; several other models might also be (rightfully) affected by adding such a duplicate while the effect on the m_j^2 would be smaller (see section 4.2)

3 Evaluation of the weighting in the perfect model test

3.1 Leave-one-out perfect model test with CMIP6

We start by calculating the performance weights in a pure model world and without using the independence weighting. In this first step we focus on the evaluation of the performance weighting when using different combinations of diagnostics and on calculating the ideal performance shape parameters (σ_D). Figure 1 shows the distribution of the CRPSS (with positive values indicating an increase in projection skill due to the weighting and vice versa; see section 2.6) evaluated for the mid- and end-of-century periods, the two SSPs, and for different combinations of diagnostics. The diagnostics range from only not-trend based (0 % tasTREND; using only tasANOM, tasSTD, pslANOM, and pslSTD) to only tasTREND based (100 % tasTREND). Overall, all diagnostic combinations tend to increase median skill compared to the unweighted projections, but there is a considerable range of CRPSS values and they can be negative. In evaluating the different cases we hence focus on two important aspects of the CRPSS distribution: (i) the median as best estimate of expected relative skill change and (ii) the 5th and 25th percentiles in particular if they are negative. Negative CRPSS values indicate a worsening of the projections compared to the unweighted case. Since the goal of the weighting is to improve the projections based on performance and dependence of the models, the risk of negative CRPSSs should be minimised.

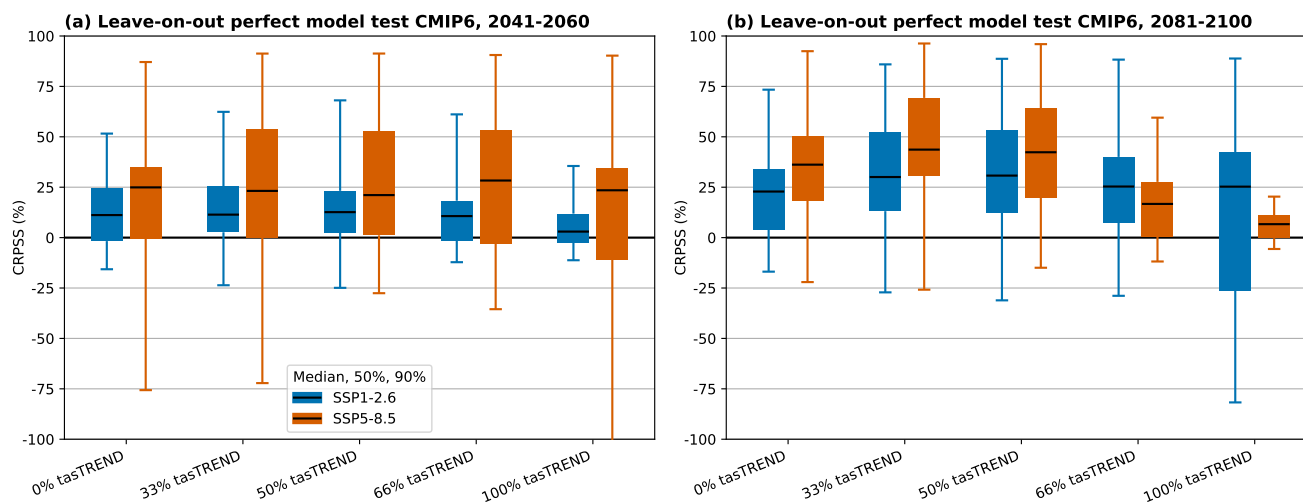


Figure 1. Continuous ranked probability skill score (CRPSS) based on a leave-one-out perfect model test with CMIP6 for (a) mid-century and (b) end-of-century temperature change relative to 1995-2014. The x-axis shows different combinations of the two diagnostic groups (see section 2.4) ranging from only not-trend based (0 % tasTREND) to only trend-based (100 % tasTREND).

We find the σ_D -values to be correctly chosen by the method in order to limit the risk for a strong skill decrease (CRPSS is close to zero or positive for the 25th percentile in almost all cases). For the mid-century period, the median skill increases by about 10 % to 20 % across both SSPs and all combination of diagnostics. The magnitude of potential negative CRPSSs in a “worst-case” scenario (5th percentile), however, is better constrained using a balanced combination of diagnostics (e.g., 50 % tasTREND). In the end-of-century period, the median skill is more variable (mainly due to the selected performance shape parameters σ_D ; see table S1), with combinations that include both trend and not-trend diagnostics again performing best.

Using 50 % tasTREND and 50 % anomaly- and variance-based diagnostics (tasANOM, tasSTD, psANOM, psLSTD) optimises the combination of median CRPSS increases and avoidance of possible negative CRPSSs; we therefore use this combination to calculate the weights for the rest of the analysis. Note that the two SSPs and time periods have slightly different σ_D values (ranging from 0.35 to 0.58; table S1), leading to slightly differing weights even though the historical information is the same. This arises from differences in confidence when applying the method for different targets. However, since the σ_D values are found to be so similar we use the mean value from the two SSPs and time periods in the following for simplicity, hence $\sigma_D = 0.43$. This does not have a strong influence on the results but simplifies their presentation and interpretation.

3.2 Perfect model test using CMIP5 as pseudo-observations

We now use each of the 27 CMIP5 models in turn as pseudo-observation and include both the performance and independence parts of the method. For all considerations in this section we use the CMIP5 merged historical and RCP runs corresponding to the CMIP6 historical and SSP runs, i.e., RCP2.6 to SSP1-2.6 and RCP8.5 to SSP5-8.5. This allows an evaluation of the skill of the weighting method applied to the full CMIP6 MME in the future. Figure 2 shows two cases selected to lead to the

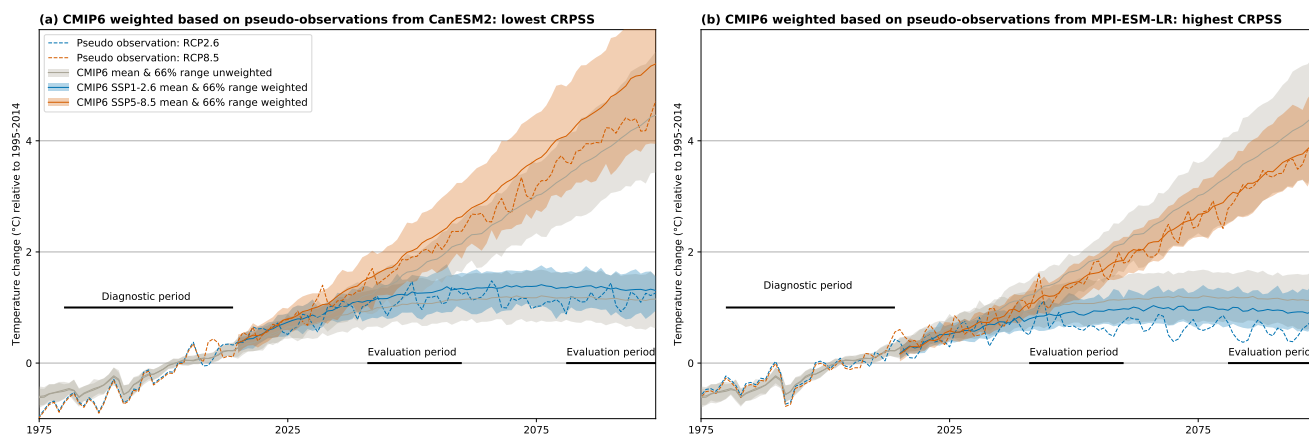


Figure 2. Time series of temperature change (relative to 1995-2014) for unweighted (gray) and weighted (colored) CMIP6 mean (lines) and likely (66 %) range (shading) as well as the CMIP5 models serving as pseudo-observations (dashed lines). Shown are the cases which lead to (a) the largest decrease in skill (CMIP5 pseudo-observation: CanESM2) and (b) to the largest increase (MPI-ESM-LR) for SSP5-8.5 in the end-of-century period. Note that no inference on the performance of the CMIP5 models can be drawn from this figure.

largest decrease (figure 2a) and increase (figure 2b) in the CRPSS for SSP5-8.5 in the end-of-century period when applying the weights. The figures reveal an important feature of the weighting: if the unweighted MME is already close to the “truth” the risk for a skill decrease is highest (figure 2a). In other words, using the CMIP5 model CanESM2, which happens to be close to the unweighted CMIP6 MME mean, as pseudo-observations to weigh CMIP6 tends to pull the CMIP6 MME mean away from the pseudo-observational “truth”. In the reverse case, if the “truth” is very different from the MME mean – e.g., the CMIP5 model MPI-ESM-LR being rather different from the CMIP6 MME mean –, the potential for a skill increase is highest (figure 2b). An important cautionary takeaway is thus to not only maximise median skill increase when setting up the method, as the cases with highest skill might come from rather “unrealistic” pseudo-observations (i.e., the ones on the tails of the model distribution, like illustrated in figure 2 and figure S1). However, in many cases we do not necessarily expect the real climate to follow such an extreme trajectory but rather be closer to the unweighted MME mean (in part because real observations tend to be used in model development and tuning). It is thus important to use a balanced set of multiple diagnostics, which might make the highest possible skill increases unattainable, but – maybe more importantly – guard against even more substantial skill decreases. An overview of the weighting based on each of the 27 CMIP5 models can be found in figure S1 in the supplement.

To look into the skill change more quantitatively, figure 3a shows the skill distribution of weighting CMIP6 to predict each of the pseudo-observations drawn from CMIP5 for both time periods and scenarios. Compared to the leave-one-out perfect model test with CMIP6 shown in figure 1 the increase in median CRPSS is lower and the risk for negative CRPSSs is slightly higher. This is not unexpected for a test sample, which has not been used for training (i.e., the estimation of the σ_D -value) and is structurally different from CMIP6 in several aspects (such as forcing scheme and maximum amount of warming). But the setup still achieves a median CRPSS increase of about 10 % to 20 %, with the risk of a skill reduction being mostly confined

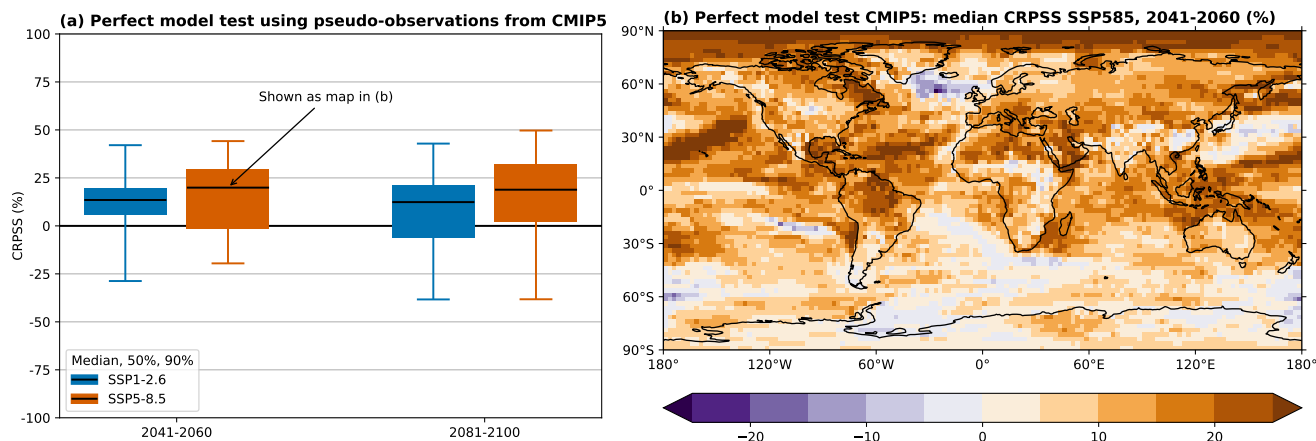


Figure 3. (a) Similar to figure 1 but using 27 CMIP5 models as pseudo-observations and showing only the 50 % tasTREND case. (b) Map of median of CRPSS values for 2041-2060 under SSP5-8.5

285 to less than 25 %, clearly showing that ClimWIP can be used to provide reliable estimates of future global temperature change and related uncertainties from the CMIP6 MME.

Finally, we consider the question of whether there are regional patterns in the skill change by investigating a map of median CRPSSs for SSP5-8.5 in the mid-century period in figure 3b (see figure S2 in the supplement for the other cases). Note that each CMIP6 model is still assigned only one weight, but the CRPSS is calculated at each grid point separately. The skill
290 increases almost everywhere with the northern hemisphere having a slightly higher amplitude. A notable exception is the North Atlantic, where weighting leads to a slight decrease in median skill. Indeed, this is the only region where the unweighted CMIP6 mean underestimates the warming from CMIP5. Weighting the CMIP6 ensemble leads to a slight strengthening of the underestimation in this region, while it reduces the difference almost everywhere else.

In summary, weighting CMIP6 in a perfect model test using five different diagnostics to establish model performance and
295 two diagnostics for independence shows an increase in skill compared to the unweighted distribution for the vast majority of cases and consistent over both investigated scenarios and time periods. Looking into the geographical distribution reveals an increase in skill almost everywhere, with some decreases found in the Southern Ocean, particularly in SSP1-2.6 (figure S2). Importantly, skill increases almost everywhere over land, thus benefiting assessments of climate impacts and adaptation where people are affected most directly.

300 4 Weighting CMIP6 projections of future warming based on observations

So far we have selected a combination of diagnostics, which leads to the highest increase in median skill while minimising the risk for a skill decrease based on an out-of-sample perfect model test with CMIP6 in section 3.1. We also argued that we use the same shape parameters (which determine the strength of the weighting) for all cases, namely $\sigma_S = 0.54$ for independence

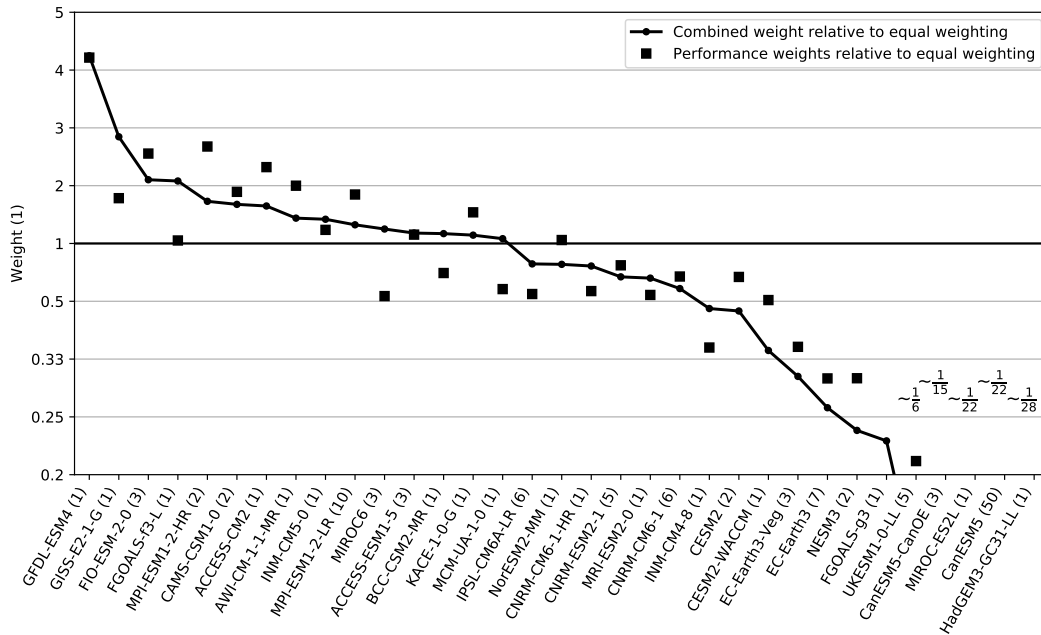


Figure 4. Combined independence-performance weights for each CMIP6 model (line with dots) and pure performance weights (squares) relative to equal weighing. Weights smaller than 0.2 times equal weighting are only shown as their approximate combined weight (fractions in the right bottom corner). The number of ensemble members per model is shown in brackets after the model name in the x-axis labels.

and $\sigma_D = 0.43$ for performance. In section 3.2 we then evaluated this setup by using pseudo-observations drawn from the
 305 CMIP5 MME. In this section we now calculate weights for CMIP6 based on observed climate and validate the effect of the independence weighting.

We use observational surface air temperature and sea level pressure estimates from the ERA5 and MERRA2 reanalyses to calculate the performance diagnostics (tasANOM, tasSTD, tasTREND, pslANOM, pslSTD). The combination of two reanalysis products allows to account for observational uncertainty, which has been found to be important for robust weighting in
 310 earlier work by Brunner et al. (2019) and Lorenz et al. (2018). As independence diagnostics we continue to use model-model distances in tasCLIM and pslCLIM.

4.1 Calculation of weights for CMIP6

Figure 4 shows the combined performance and independence weights assigned to each CMIP6 model by ClimWIP when applied to the target of global temperature change. Three general regimes can be identified: (i) models which represent historical
 315 observations better than average receive relative weights mostly between 1 and 2 (with a maximum of about 4), (ii) models which represent historical observations slightly less well, but can still be considered skillful representations of the climate system, receive relative weights mostly between 1 and 0.5, and (iii) models which can be considered less skillful based on their past performance receive weights of less than 0.2.

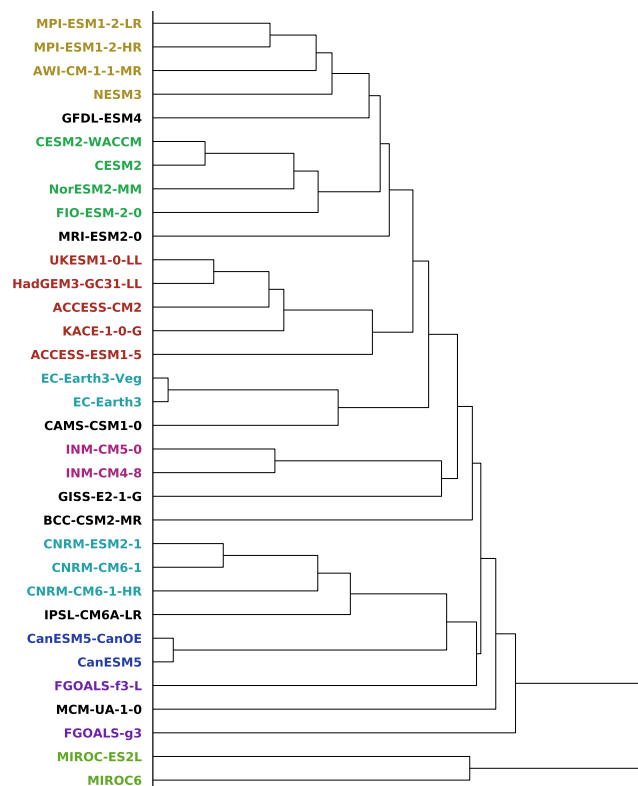


Figure 5. Model “family tree” for all 33 CMIP6 models used in this study similar to Knutti et al. (2013). Based on global, horizontally resolved tasCLIM and pslCLIM in the period 1980-2014. Labels with the same colour indicate models with obvious dependencies such as shared components or same origin (models with no clear dependencies are labelled in black). Weak relations such as remote “ancestors” are not colored together (e.g., BCC-CSM2-MR and CESM2).

In addition, figure 4 also shows the pure performance weights. The relative differences to the combined weights are mostly below 50 %, with the MIROC model family being one notable exception. Both MIROC models are very independent, which shifts MIROC6 from a below-average model (based on the pure performance weight; black square in figure 4) to an above-average model in the combined weight (black dot) effectively more than doubling its performance weight. For MIROC-ES2L the scaling due to independence is similarly high (not visible in figure 4), but its total weight is still dominated by the very low performance weight. In the next section we investigate if these independence weights indeed correctly represent the complex model inter-dependencies in the CMIP6 MME and down-weight models which are highly dependent on other models appropriately.

4.2 Validation of the independence weighting

To test if model inter-dependence can correctly be inferred from model output in general, we first take a quantitative approach, somewhat different to the model (independence) weighting itself. Using the same two diagnostics, namely horizontally re-

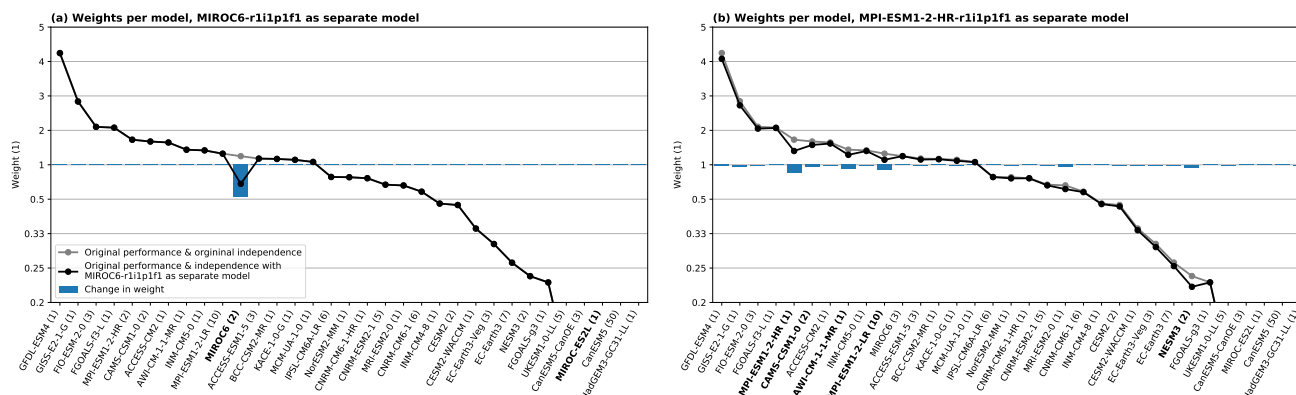


Figure 6. Similar to figure 4 but removing one variant from (a) MIROC6 and (b) MPI-ESM1-2-HR and adding it as separate model when calculating the independence weights (the “new” model is not shown in the plot). Models with obvious dependencies to the “new” model (same as in figure 5) have bold labels.

330 solved global temperature and sea level pressure climatologies (from 1980-2014) we apply a hierarchical clustering approach (section 2.7). Figure 5 shows the resulting “family tree” of CMIP6 models similar to the work by Masson and Knutti (2011) and Knutti et al. (2013). Models with the same origin or known shared components are marked in the same colour, as this is the most objective measure for a priori model dependence we have. The information about the model components is taken from each models description page on the ES-DOC explorer (<https://es-doc.org/cmip6/>) as listed in table S3 in the supplement. Figure 5 shows that clustering models based on the selected diagnostics performs well: related models such as low and high resolution versions (MPI-ESM-2-LR and MPI-ESM-2-HR; CNRM-CM6-1 and CNRM-CM6-1-HR) or versions with only one differing component (CESM2 and CESM2-WACCM; INM-CM5-0 and INM-CM4-8; both differing only in the atmosphere) are detected as being very similar. Both MIROC models, which have been identified as very independent based on figure 4 are again found to be very far away from each other and even further away from all other models in the CMIP6 MME.

340 To investigate if the independence weighting correctly identifies and weights models based on their degree of inter-dependence we now look at two models as examples: one model that performs well and is relatively independent (MIROC6) and another that also performs well but is more dependent (MPI-ESM1-2-HR). Each has multiple ensemble members; we remove one member from each and add it to the MME as an additional model as detailed in section 2.7.

In the first case (figure 6a; MIROC6 which is among the least dependent models), the original weight is reduced by almost 1/2, which is close to what we would expect in the idealised case. All other models are unaffected by adding a duplicate of MIROC6, even the other model from the same center, MIROC-ES2L which differs in atmospheric resolution and cumulus treatment (Tatebe et al., 2019; Hajima et al., 2019). Based on the “family tree” shown in figure 5 this behaviour is not surprising: the two MIROC models are not only identified as the most independent models in the CMIP6 MME but also as very independent from each. While some of the components and parameterizations are similar, updates in parameterizations and in the tuning of the parameters appear to be sufficient here to create a model that behaves quite differently.

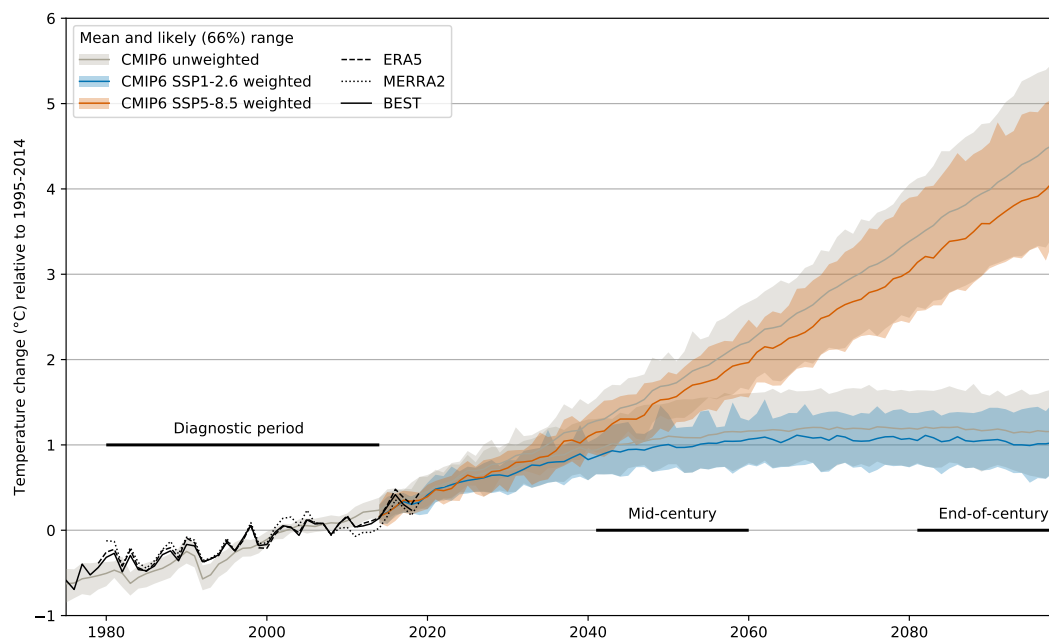


Figure 7. Timeseries of temperature change (relative to 1995-2014) for unweighted (gray) and weighted (colored) CMIP6 mean (lines) and likely (66 %) range (shading). Three observational datasets are also shown in black; note that BEST is not used to inform the weighting and is only shown for comparison here.

The second case (figure 6b; MPI-ESM1-2-HR which is among the most dependent models) shows a very different picture. The strongest effect on the original weight is found for the copied model itself, which is reduced by about 0.8, but also several other models are affected: MPI-ESM1-2-LR (reduced by 0.86), AWI-CM-1-1-MR (0.9), NESM3 (0.93), MRI-ESM2-0 (0.94), and CAMS-CSM1-0 (0.94). Looking into these models in more detail, we conclude that the inter-dependencies
355 detected by our method can be traced to shared components in most cases: MPI-ESM1-2-LR is just the low resolution version of MPI-ESM1-2-HR (run with a T63 atmosphere instead of T127 and a 1.5° ocean instead of 0.4°), AWI-CM-1-1-MR and NESM3 share the atmospheric (ECHAM6.3) and similar land (JSBACH3.x) components, and CAMS-CSM1-0 shares a similar atmospheric (ECHAM5) component, while MRI-ESM2-0 does not have any obvious dependencies. Information about the models can be found in their reference publications (Mauritsen et al., 2019; Gutjahr et al., 2019; Semmler et al., 2019; Yang
360 et al., 2020; Chen et al., 2019; Yukimoto et al., 2019) and on the ES-DOC explorer, which provides detailed information about all model used in this study. The links to each models information page can be found in table S3 in the supplementary material.

4.3 Applying weights to CMIP6 temperature projections and TCR

Figure 7 shows a timeseries of unweighted and weighted projections based on a weak (SSP1-2.6) and strong (SSP5-8.5) climate change scenario. For both scenarios a clear shift in the mean towards less warming is visible, which is also reflected in the
365 upper uncertainty bound. Notably, however, the lower bound hardly changes, leading to a reduction in projection uncertainty

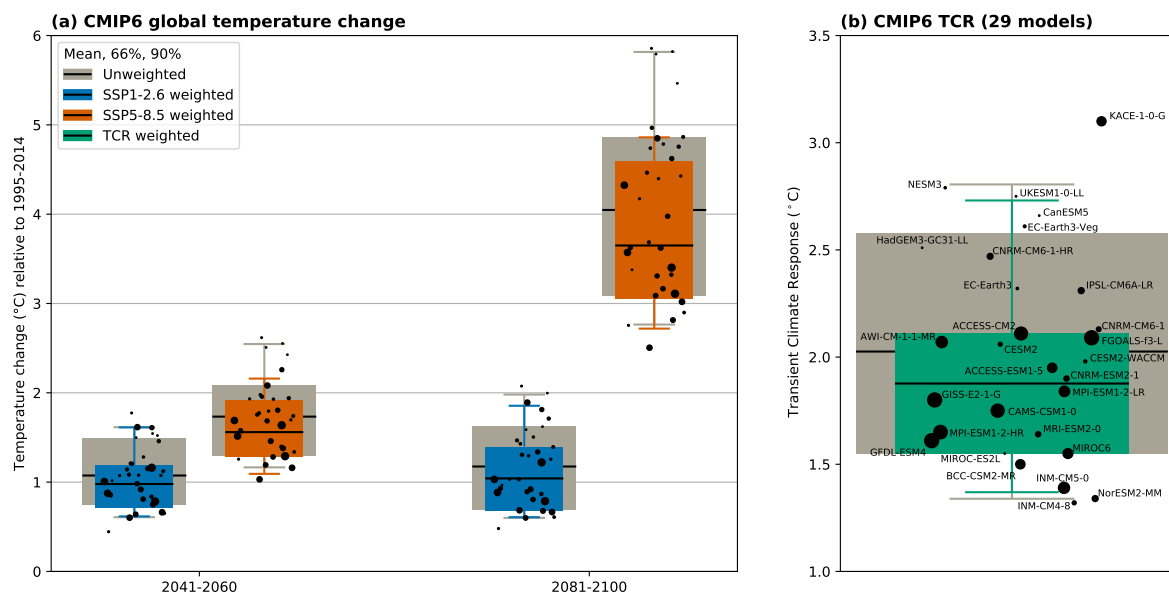


Figure 8. (a) Unweighted (gray) and weighted (colors) temperature change (relative to 1995-2014) for both periods and scenarios. (b) Unweighted (gray) and weighted (green) Transient Climate Response (TCR). The dots show individual models as labelled, with the dot size indicating the weight. The horizontal dot position is arbitrary.

in total. This becomes even clearer when investigating the two 20-year periods, reflecting mid- and end-of-century conditions (figure 8a and table S2).

Based on these results, warming exceeding 5 °C by the end of the century is very unlikely even under the strongest climate change scenario SSP5-8.5. The mean warming for this case is shifted downward to about 3.7 °C and the 66 % (likely) and 90 %
 370 ranges are reduced by 12 % and 30 %, respectively. For SSP1-2.6 in the end-of-century period as well as both SSPs in the mid-century period, reductions in the mean warming of about 0.1 °C are found. The likely range is reduced by about 30 % in these three cases. A summary of all statistics can be found in table S2 in the supplement. Recent studies that use historical temperature trend as an observational constraint for future warming lead to similar conclusions, with lower constrained warming compared to unconstrained (both in the mean and upper percentiles of the distributions) (e.g., Tokarska et al., 2020; Nijse et al., 2020).

375 To investigate the influence of remaining internal variability in our combination of diagnostics on the weighting we also perform a bootstrap test. Selecting only one random member per model (for models with more than one ensemble member) we calculate weights and the corresponding unweighted and weighted temperature change distributions. This is repeated 100 times, providing uncertainty estimates for both the unweighted and weighted percentiles. The mean values of the weighted percentiles taken over all 100 bootstrap samples are very similar to the values from the weighting based on the full MME
 380 (including all ensemble members; see figure S3) confirming the robustness of our approach.

We also apply weights to TCR estimates in figure 8b. For four models included in the weighting of temperature change we do not yet have all information available to estimate TCR (FGOALS-g3, CanESM5-CanOE, FIO-ESM-2-0, MCM-UA-1-0);



these are omitted in figure 8b. For the remaining 29 models we find a unweighted mean TCR value of about 2 °C with a likely range of 1.6 °C to 2.6 °C. Weighting by historical model performance and independence constrains this to 1.9 °C (1.6 °C to 385 2.1 °C), a reduction of 46 % in the likely range. These values are consistent with recent studies based on emergent constraints which estimate the likely range of TCR to be 1.5 °C to 2.2 °C (Nijssen et al., 2020) and 1.2 °C to 2.0 °C (Tokarska et al., 2020). They are also consistent but substantially more narrow than the likely range from the fifth assessment report of the IPCC (IPCC, 2013) based on CMIP5: 1 °C to 2.5 °C.

Figure 8b clearly shows that almost all models with higher than equal weights lie within the likely range, and only one model 390 lies above it (KACE-1-0-G). This is a strong indication that TCR values beyond about 2.5 °C are unlikely when weighting based on several diagnostics and when accounting for model independence. The weighting also largely reconciles CMIP6 with 5 by giving less weight to some of the models in CMIP6 that warm most strongly.

5 Discussion and Conclusions

We have used the Climate model Weighting by Independence and Performance (ClimWIP) method to constrain projections 395 of future global temperature change from the CMIP6 multi-model ensemble. Based on a leave-one-out perfect model test, a combination of five global, horizontally-resolved diagnostic fields (anomaly, variance, and trend of surface air temperature and anomaly and variance of sea level pressure) was selected to inform the performance weighting. The skill of weighting based on this selection was tested and confirmed in a second perfect model test using CMIP5 models as pseudo-observations. Our results clearly show the usefulness of this weighting approach in translating model spread into reliable estimates of future changes 400 and in particular into uncertainties that are consistent with observations of present day climate and observed trends.

We also discussed the remaining risk for decreasing skill compared to the raw distribution which is a crucial question in all weighting or constraining methods. We show the importance of using a balanced combination of climate system features (i.e., diagnostics) relevant for the target to inform the weighting to minimise the risk for skill decreases. This guards against the possibility of a model “accidentally” fitting observations for a single diagnostic while being far away from them in several 405 others (and hence possibly not providing a skilful projection of the target variable).

By adding copies of existing models into the CMIP6 multi-model ensemble we verified the effect of the independence weighting, showing that models get correctly down-weighted based on an estimate of dependence derived from their output. To inform the independence weighting we used two global, horizontally resolved fields (climatology of surface air temperature and sea level pressure) which we showed to allow a clear clustering of models with obvious inter-dependencies using a CMIP6 410 “family tree”.

From these tests we conclude that ClimWIP is skilful in weighting global mean temperature change from CMIP6 using the selected setup. We hence use it to calculate weights for each CMIP6 model and apply them in order to obtain probabilistic estimates of future changes. Compared to the unweighted case these results clearly show that the CMIP6 models which lead to the highest warming are less probable, confirming earlier studies (e.g., Tokarska et al., 2020; Nijssen et al., 2020). We find 415 a weighted mean global temperature change (relative to 1995-2014) of 3.7 °C with a likely (66 %) range of 3.1 °C to 4.6 °C



by the end of the century when following SSP5-8.5. With ambitious climate mitigation (SSP1-2.6) a weighted mean change of 1 °C (likely range: 0.7 °C to 1.4 °C) is projected for the same period.

On the policy level, this highlights the need for quick and decisive climate action to achieve the Paris climate targets. For climate modeling on the other hand, this approach demonstrates the potential to narrow the uncertainties in CMIP6 projections, particular on the upper bound. The large investments in climate model development have so far not led to reduced model spread in the raw ensemble, but the use of climatological information and emergent transient constraints has the potential to provide more robust projections with reduced uncertainties, that at the same time are more consistent with observed trends, thus maximizing the value of climate model information for impacts and adaptation.

Code availability. The ClimWIP model weighting package is available under a GPLv3 at <https://github.com/lukasbrunner/ClimWIP.git>

Author contributions. LB, ALM, and RK were involved in conceiving the study. LB did the analysis and created the plots substantially supported by AGP. LB wrote the manuscript with contributions from all authors. The ClimWIP package was implemented by LB and RL; AGP wrote the script used to create tables S3 and S5.

Competing interests. The authors declare that they have no conflict of interest.

Acknowledgements. The authors thank Martin B. Stolpe for providing the TCR values and Katarzyna B. Tokarska for helpful discussions and comments on the manuscript. The EUCP project is funded by the European Commission through the Horizon 2020 Programme for Research and Innovation: Grant Agreement 776613. Ruth Lorenz was funded by the European Union's Horizon 2020 Research and Innovation program: Grant Agreement 641816 (CRESCENDO). Flavio Lehner is supported by a Swiss NSF Ambizione Fellowship (Project PZ00P2_174128). This material is partly based upon work supported by the National Center for Atmospheric Research, which is a major facility sponsored by the National Science Foundation (NSF) under Cooperative Agreement No. 1947282, and by the Regional and Global Model Analysis (RGMA) component of the Earth and Environmental System Modeling Program of the U.S. Department of Energy's Office of Biological & Environmental Research (BER) via NSF IA 1844590. This study was generated using Copernicus Climate Change Service Information 2020 from ERA5. The authors thank NASA for providing MERRA2 and Berkeley Earth for providing BEST. We acknowledge the World Climate Research Programme, which, through its Working Group on Coupled Modelling, coordinated and promoted CMIP5 and 6. We thank the climate modeling groups for producing and making available their model output, the Earth System Grid Federation (ESGF) for archiving the data and providing access, and the multiple funding agencies who support CMIP5 and 6 and ESGF. We thank all contributors to the numerous Python packages which were crucial for this work, in particular the xarray project (<http://xarray.pydata.org>).



References

- Amos, M., Young, P. J., Hosking, J. S., Lamarque, J.-F., Abraham, N. L., Akiyoshi, H., Archibald, A. T., Bekki, S., Deushi, M., Jöckel, P., Kinnison, D., Kirner, O., Kunze, M., Marchand, M., Plummer, D. A., Saint-Martin, D., Sudo, K., Tilmes, S., and Yamashita, Y.:
445 Projecting ozone hole recovery using an ensemble of chemistry-climate models weighted by model performance and independence, *Atmospheric Chemistry and Physics Discussions*, 2020, 1–26, <https://doi.org/10.5194/acp-2020-86>, <https://www.atmos-chem-phys-discuss.net/acp-2020-86/>, 2020.
- Andrews, T., Andrews, M. B., Bodas-Salcedo, A., Jones, G. S., Kuhlbrodt, T., Manners, J., Menary, M. B., Ridley, J., Ringer, M. A., Sellar, A. A., Senior, C. A., and Tang, Y.: Forcings, Feedbacks, and Climate Sensitivity in HadGEM3-GC3.1 and UKESM1, *Journal of Advances in Modeling Earth Systems*, 11, 4377–4394, <https://doi.org/10.1029/2019MS001866>, 2019.
450
- Annan, J. D. and Hargreaves, J. C.: On the meaning of independence in climate science, *Earth System Dynamics*, 8, 211–224, <https://doi.org/10.5194/esd-8-211-2017>, 2017.
- Bishop, C. H. and Abramowitz, G.: Climate model dependence and the replicate Earth paradigm, *Climate Dynamics*, 41, 885–900, <https://doi.org/10.1007/s00382-012-1610-y>, 2013.
- 455 Boé, J.: Interdependency in Multimodel Climate Projections: Component Replication and Result Similarity, *Geophysical Research Letters*, 45, 2771–2779, <https://doi.org/10.1002/2017GL076829>, <http://doi.wiley.com/10.1002/2017GL076829>, 2018.
- Boé, J. and Terray, L.: Can metric-based approaches really improve multi-model climate projections? The case of summer temperature change in France, *Climate Dynamics*, 45, 1913–1928, <https://doi.org/10.1007/s00382-014-2445-5>, 2015.
- Brunner, L., Lorenz, R., Zumwald, M., and Knutti, R.: Quantifying uncertainty in European climate projections using combined performance-independence weighting, *Environmental Research Letters*, 14, 124010, <https://doi.org/10.1088/1748-9326/ab492f>, <http://dx.doi.org/10.1038/ngeo3017>, 2019.
460
- Brunner, L., Hauser, M., Lorenz, R., and Beyerle, U.: The ETH Zurich CMIP6 next generation archive : technical documentation, <https://doi.org/10.5281/zenodo.3734128>, 2020a.
- Brunner, L., McSweeney, C., Bafort, D. J., O'Reilly, C., Booth, B., Harris, G., Lowe, J., Benassi, M., Coppola, E., Nogherotto, R., Hegerl, G. C., Knutti, R., Lenderink, G., de Vries, H., Qasmi, S., Ribes, A., and Undorf, S.: Quantifying uncertainty in projections of future European climate: a multi-model multi-method approach, *Journal of Climate*, 2020b.
465
- C3S: ERA5: Fifth generation of ECMWF atmospheric reanalyses of the global climate, <https://doi.org/10.24381/cds.f17050d7>, accessed: 26.3.2020, 2017.
- Chen, X., Guo, Z., Zhou, T., Li, J., Rong, X., Xin, Y., Chen, H., and Su, J.: Climate Sensitivity and Feedbacks of a New Coupled
470 Model CAMS-CSM to Idealized CO₂ Forcing: A Comparison with CMIP5 Models, *Journal of Meteorological Research*, 33, 31–45, <https://doi.org/10.1007/s13351-019-8074-5>, 2019.
- Eyring, V., Bony, S., Meehl, G. A., Senior, C. A., Stevens, B., Stouffer, R. J., and Taylor, K. E.: Overview of the Coupled Model Intercomparison Project Phase 6 (CMIP6) experimental design and organization, *Geoscientific Model Development*, 9, 1937–1958, <https://doi.org/10.5194/gmd-9-1937-2016>, <https://www.geosci-model-dev.net/9/1937/2016/>, 2016.
- 475 Eyring, V., Cox, P. M., Flato, G. M., Gleckler, P. J., Abramowitz, G., Caldwell, P., Collins, W. D., Gier, B. K., Hall, A. D., Hoffman, F. M., Hurtt, G. C., Jahn, A., Jones, C. D., Klein, S. A., Krasting, J. P., Kwiatkowski, L., Lorenz, R., Maloney, E., Meehl, G. A., Pendergrass, A. G., Pincus, R., Ruane, A. C., Russell, J. L., Sanderson, B. M., Santer, B. D., Sherwood, S. C., Simpson, I. R., Stouffer, R. J., and



- Williamson, M. S.: Taking climate model evaluation to the next level, *Nature Climate Change*, 9, 102–110, <https://doi.org/10.1038/s41558-018-0355-y>, <http://dx.doi.org/10.1038/s41558-018-0355-y>, 2019.
- 480 Flato, G., Marotzke, J., Abiodun, B., Braconnot, P., Chou, S., Collins, W., Cox, P., Driouech, F., Emori, S., Eyring, V., Forest, C., Gleckler, P., Guilyardi, E., Jakob, C., Kattsov, V., Reason, C., and Rummukainen, M.: Evaluation of Climate Models, in: *Climate Change 2013: The Physical Science Basis. Contribution of Working Group I to the Fifth Assessment Report of the Intergovernmental Panel on Climate Change*, edited by Stocker, T., Qin, D., Plattner, G.-K., Tignor, M., Allen, S., Boschung, J., Nauels, A., Xia, Y., Bex, V., and Midgley, P., Cambridge University Press, Cambridge, United Kingdom and New York, NY, USA, 2013.
- 485 Forster, P. M., Andrews, T., Good, P., Gregory, J. M., Jackson, L. S., and Zelinka, M.: Evaluating adjusted forcing and model spread for historical and future scenarios in the CMIP5 generation of climate models, *Journal of Geophysical Research Atmospheres*, 118, 1139–1150, <https://doi.org/10.1002/jgrd.50174>, 2013.
- Forster, P. M., Maycock, A. C., McKenna, C. M., and Smith, C. J.: Latest climate models confirm need for urgent mitigation, *Nature Climate Change*, 10, 7–10, <https://doi.org/10.1038/s41558-019-0660-0>, 2020.
- 490 Gelaro, R., McCarty, W., Suárez, M. J., Todling, R., Molod, A., Takacs, L., Randles, C. A., Darmenov, A., Bosilovich, M. G., Reichle, R., Wargan, K., Coy, L., Cullather, R., Draper, C., Akella, S., Buchard, V., Conaty, A., da Silva, A. M., Gu, W., Kim, G. K., Koster, R., Lucchesi, R., Merkova, D., Nielsen, J. E., Partyka, G., Pawson, S., Putman, W., Rienecker, M., Schubert, S. D., Sienkiewicz, M., and Zhao, B.: The modern-era retrospective analysis for research and applications, version 2 (MERRA-2), *Journal of Climate*, 30, 5419–5454, <https://doi.org/10.1175/JCLI-D-16-0758.1>, 2017.
- 495 Gettelman, A., Hannay, C., Bacmeister, J. T., Neale, R. B., Pendergrass, A. G., Danabasoglu, G., Lamarque, J., Fasullo, J. T., Bailey, D. A., Lawrence, D. M., and Mills, M. J.: High Climate Sensitivity in the Community Earth System Model Version 2 (CESM2), *Geophysical Research Letters*, 46, 8329–8337, <https://doi.org/10.1029/2019GL083978>, <https://onlinelibrary.wiley.com/doi/abs/10.1029/2019GL083978>, 2019.
- Giorgi, F. and Coppola, E.: Does the model regional bias affect the projected regional climate change? An analysis of global model projections: A letter, *Climatic Change*, 100, 787–795, <https://doi.org/10.1007/s10584-010-9864-z>, 2010.
- 500 Giorgi, F. and Mearns, L. O.: Calculation of average, uncertainty range, and reliability of regional climate changes from AOGCM simulations via the "Reliability Ensemble Averaging" (REA) method, *Journal of Climate*, 15, 1141–1158, [https://doi.org/10.1175/1520-0442\(2002\)015<1141:COAURA>2.0.CO;2](https://doi.org/10.1175/1520-0442(2002)015<1141:COAURA>2.0.CO;2), 2002.
- GMAO: MERRA-2 tavg1_2d_slv_Nx: 2d,1-Hourly,Time-Averaged,Single-Level,Assimilation,Single-Level Diagnostics V5.12.4, <https://disc.gsfc.nasa.gov/api/jobs/results/5e7b68e9ed720b5795af914a>, accessed: 25.3.2020, 2015a.
- 505 GMAO: MERRA-2 statD_2d_slv_Nx: 2d,Daily,Aggregated Statistics,Single-Level,Assimilation,Single-Level Diagnostics V5.12.4, <https://disc.gsfc.nasa.gov/api/jobs/results/5e7b648f4900ab500326d17e>, accessed: 25.3.2020, 2015b.
- Golaz, J. C., Caldwell, P. M., Van Roekel, L. P., Petersen, M. R., Tang, Q., Wolfe, J. D., Abeshu, G., Anantharaj, V., Asay-Davis, X. S., Bader, D. C., Baldwin, S. A., Bisht, G., Bogenschutz, P. A., Branstetter, M., Brunke, M. A., Brus, S. R., Burrows, S. M., Cameron-Smith, P. J., Donahue, A. S., Deakin, M., Easter, R. C., Evans, K. J., Feng, Y., Flanner, M., Foucar, J. G., Fyke, J. G., Griffin, B. M., Hannay, C., Harrop, B. E., Hoffman, M. J., Hunke, E. C., Jacob, R. L., Jacobsen, D. W., Jeffery, N., Jones, P. W., Keen, N. D., Klein, S. A., Larson, V. E., Leung, L. R., Li, H. Y., Lin, W., Lipscomb, W. H., Ma, P. L., Mahajan, S., Maltrud, M. E., Mamtjanov, A., McClean, J. L., McCoy, R. B., Neale, R. B., Price, S. F., Qian, Y., Rasch, P. J., Reeves Eyre, J. E., Riley, W. J., Ringler, T. D., Roberts, A. F., Roesler, E. L., Salinger, A. G., Shaheen, Z., Shi, X., Singh, B., Tang, J., Taylor, M. A., Thornton, P. E., Turner, A. K., Veneziani, M., Wan, H., Wang, H., Wang, S., Williams, D. N., Wolfram, P. J., Worley, P. H., Xie, S., Yang, Y., Yoon, J. H., Zelinka, M. D., Zender, C. S., Zeng, X., Zhang, C.,
- 515



- Zhang, K., Zhang, Y., Zheng, X., Zhou, T., and Zhu, Q.: The DOE E3SM Coupled Model Version 1: Overview and Evaluation at Standard Resolution, *Journal of Advances in Modeling Earth Systems*, 11, 2089–2129, <https://doi.org/10.1029/2018MS001603>, 2019.
- Gutjahr, O., Putrasahan, D., Lohmann, K., Jungclaus, J. H., Von Storch, J. S., Brüggemann, N., Haak, H., and Stössel, A.: Max Planck Institute Earth System Model (MPI-ESM1.2) for the High-Resolution Model Intercomparison Project (HighResMIP), *Geoscientific Model Development*, 12, 3241–3281, <https://doi.org/10.5194/gmd-12-3241-2019>, 2019.
- Hajima, T., Watanabe, M., Yamamoto, A., Tatebe, H., Noguchi, M., Abe, M., Ohgaito, R., Ito, A., Yamazaki, D., Okajima, H., Ito, A., Takata, K., Ogochi, K., Watanabe, S., and Kawamiya, M.: Description of the MIROC-ES2L Earth system model and evaluation of its climate–biogeochemical processes and feedbacks, *Geoscientific Model Development Discussions*, 5, 1–73, <https://doi.org/10.5194/gmd-2019-275>, 2019.
- Hawkins, E. and Sutton, R.: The Potential to Narrow Uncertainty in Regional Climate Predictions, *Bulletin of the American Meteorological Society*, 90, 1095–1108, <https://doi.org/10.1175/2009BAMS2607.1>, <http://journals.ametsoc.org/doi/10.1175/2009BAMS2607.1>, 2009.
- Hersbach, H.: Decomposition of the Continuous Ranked Probability Score for Ensemble Prediction Systems, *Weather and Forecasting*, 15, 559–570, [https://doi.org/10.1175/1520-0434\(2000\)015<0559:DOTCRP>2.0.CO;2](https://doi.org/10.1175/1520-0434(2000)015<0559:DOTCRP>2.0.CO;2), <http://journals.ametsoc.org/doi/abs/10.1175/1520-0434%282000%29015%3C0559%3ADOTCRP%3E2.0.CO%3B2>, 2000.
- IPCC: Climate Change 2013: The Physical Science Basis. Contribution of Working Group I to the Fifth Assessment Report of the Intergovernmental Panel on Climate Change [Stocker,., 9, Cambridge University Press, 2013.
- Jiménez-de-la Cuesta, D. and Mauritsen, T.: Emergent constraints on Earth’s transient and equilibrium response to doubled CO₂ from post-1970s global warming, *Nature Geoscience*, 2015, <https://doi.org/10.1038/s41561-019-0463-y>, 2019.
- Kay, J. E., Deser, C., Phillips, A., Mai, A., Hannay, C., Strand, G., Arblaster, J. M., Bates, S. C., Danabasoglu, G., Edwards, J., Holland, M., Kushner, P., Lamarque, J. F., Lawrence, D., Lindsay, K., Middleton, A., Munoz, E., Neale, R., Oleson, K., Polvani, L., and Vertenstein, M.: The community earth system model (CESM) large ensemble project : A community resource for studying climate change in the presence of internal climate variability, *Bulletin of the American Meteorological Society*, 96, 1333–1349, <https://doi.org/10.1175/BAMS-D-13-00255.1>, 2015.
- Knutti, R., Furrer, R., Tebaldi, C., Cermak, J., and Meehl, G. A.: Challenges in combining projections from multiple climate models, *Journal of Climate*, 23, 2739–2758, <https://doi.org/10.1175/2009JCLI3361.1>, 2010.
- Knutti, R., Masson, D., and Gettelman, A.: Climate model genealogy: Generation CMIP5 and how we got there, *Geophysical Research Letters*, 40, 1194–1199, <https://doi.org/10.1002/grl.50256>, 2013.
- Knutti, R., Rugenstein, M. A., and Hegerl, G. C.: Beyond equilibrium climate sensitivity, *Nature Geoscience*, 10, 727–736, <https://doi.org/10.1038/NGEO3017>, <http://dx.doi.org/10.1038/ngeo3017>, 2017a.
- Knutti, R., Sedláček, J., Sanderson, B. M., Lorenz, R., Fischer, E. M., and Eyring, V.: A climate model projection weighting scheme accounting for performance and interdependence, *Geophysical Research Letters*, 44, 1909–1918, <https://doi.org/10.1002/2016GL072012>, <http://doi.wiley.com/10.1002/2016GL072012>, 2017b.
- Lehner, F., Deser, C., Maher, N., Marotzke, J., Fischer, E., Brunner, L., Knutti, R., and Hawkins, E.: Partitioning climate projection uncertainty with multiple Large Ensembles and CMIP5/6, *Earth System Dynamics Discussions*, pp. 1–28, <https://doi.org/10.5194/esd-2019-93>, 2020.
- Lorenz, R., Herger, N., Sedláček, J., Eyring, V., Fischer, E. M., and Knutti, R.: Prospects and Caveats of Weighting Climate Models for Summer Maximum Temperature Projections Over North America, *Journal of Geophysical Research: Atmospheres*, 123, 4509–4526, <https://doi.org/10.1029/2017JD027992>, <http://doi.wiley.com/10.1029/2017JD027992>, 2018.



- Maher, N., Milinski, S., Suarez-Gutierrez, L., Botzet, M., Dobrynin, M., Kornbluh, L., Kröger, J., Takano, Y., Ghosh, R., Hedemann, C., Li, C., Li, H., Manzini, E., Notz, D., Putrasahan, D., Boysen, L., Claussen, M., Ilyina, T., Olonscheck, D., Raddatz, T., Stevens, B., and Marotzke, J.: The Max Planck Institute Grand Ensemble: Enabling the Exploration of Climate System Variability, *Journal of Advances in Modeling Earth Systems*, <https://doi.org/10.1029/2019MS001639>, 2019.
- Masson, D. and Knutti, R.: Climate model genealogy, *Geophysical Research Letters*, 38, 1–4, <https://doi.org/10.1029/2011GL046864>, 2011.
- Mauritsen, T., Bader, J., Becker, T., Behrens, J., Bittner, M., Brokopf, R., Brovkin, V., Claussen, M., Crueger, T., Esch, M., Fast, I., Fiedler, S., Fläschner, D., Gayler, V., Giorgetta, M., Goll, D. S., Haak, H., Hagemann, S., Hedemann, C., Hohenegger, C., Ilyina, T., Jahns, T., Jimenez-de-la Cuesta, D., Jungclaus, J., Kleinen, T., Kloster, S., Kracher, D., Kinne, S., Kleberg, D., Lasslop, G., Kornbluh, L., Marotzke, J., Matei, D., Meraner, K., Mikolajewicz, U., Modali, K., Möbis, B., Müller, W. A., Nabel, J. E., Nam, C. C., Notz, D., Nyawira, S. S., Paulsen, H., Peters, K., Pincus, R., Pohlmann, H., Pongratz, J., Popp, M., Raddatz, T. J., Rast, S., Redler, R., Reick, C. H., Rohrschneider, T., Schemann, V., Schmidt, H., Schnur, R., Schulzweida, U., Six, K. D., Stein, L., Stemmler, I., Stevens, B., von Storch, J. S., Tian, F., Voigt, A., Vrese, P., Wieners, K. H., Wilkenskeld, S., Winkler, A., and Roeckner, E.: Developments in the MPI-M Earth System Model version 1.2 (MPI-ESM1.2) and Its Response to Increasing CO₂, *Journal of Advances in Modeling Earth Systems*, 11, 998–1038, <https://doi.org/10.1029/2018MS001400>, 2019.
- Merrifield, A. L., Brunner, L., Lorenz, R., and Knutti, R.: Weighting scheme to incorporate large ensembles in multi-model ensemble projections, *Earth System Dynamics*, <https://doi.org/10.5194/esd-2019-69>, <https://doi.org/10.5194/esd-2019-69>, 2019.
- Müllner, D.: Modern hierarchical, agglomerative clustering algorithms, pp. 1–29, <http://arxiv.org/abs/1109.2378>, 2011.
- Nijse, F. J. M. M., Cox, P. M., and Williamson, M. S.: An emergent constraint on Transient Climate Response from simulated historical warming in CMIP6 models, *Earth System Dynamics*, pp. 1–14, <https://doi.org/10.5194/esd-2019-86>, <https://doi.org/10.5194/esd-2019-86>, 2020.
- O’Neill, B. C., Kriegler, E., Riahi, K., Ebi, K. L., Hallegatte, S., Carter, T. R., Mathur, R., and van Vuuren, D. P.: A new scenario framework for climate change research: the concept of shared socioeconomic pathways, *Climatic Change*, 122, 387–400, <https://doi.org/10.1007/s10584-013-0905-2>, <http://link.springer.com/10.1007/s10584-013-0905-2>, 2014.
- Ribes, A., Zwiers, F. W., Azaïs, J. M., and Naveau, P.: A new statistical approach to climate change detection and attribution, *Climate Dynamics*, 48, 367–386, <https://doi.org/10.1007/s00382-016-3079-6>, 2017.
- Sanderson, B. M., Knutti, R., and Caldwell, P.: A representative democracy to reduce interdependency in a multimodel ensemble, *Journal of Climate*, 28, 5171–5194, <https://doi.org/10.1175/JCLI-D-14-00362.1>, 2015a.
- Sanderson, B. M., Knutti, R., and Caldwell, P.: Addressing interdependency in a multimodel ensemble by interpolation of model properties, *Journal of Climate*, 28, 5150–5170, <https://doi.org/10.1175/JCLI-D-14-00361.1>, 2015b.
- Sanderson, B. M., Wehner, M., and Knutti, R.: Skill and independence weighting for multi-model assessments, *Geoscientific Model Development*, 10, 2379–2395, <https://doi.org/10.5194/gmd-10-2379-2017>, 2017.
- Selten, F. M., Bintanja, R., Vautard, R., and van den Hurk, B. J.: Future continental summer warming constrained by the present-day seasonal cycle of surface hydrology, *Scientific Reports*, 10, 1–7, <https://doi.org/10.1038/s41598-020-61721-9>, <http://dx.doi.org/10.1038/s41598-020-61721-9>, 2020.
- Semmler, T., Danilov, S., Gierz, P., Goessling, H., Hegewald, J., Hinrichs, C., Koldunov, N. V., Khosravi, N., Mu, L., and Rackow, T.: Simulations for CMIP6 with the AWI climate model AWI-CM-1-1, *Earth and Space Science Open Archive*, p. 48, <https://doi.org/10.1002/essoar.10501538.1>, 2019.



- 590 Swart, N. C., Cole, J. N., Kharin, V. V., Lazare, M., Scinocca, J. F., Gillett, N. P., Anstey, J., Arora, V., Christian, J. R., Hanna, S., Jiao, Y., Lee, W. G., Majaess, F., Saenko, O. A., Seiler, C., Seinen, C., Shao, A., Sigmond, M., Solheim, L., Von Salzen, K., Yang, D., and Winter, B.: The Canadian Earth System Model version 5 (CanESM5.0.3), *Geoscientific Model Development*, 12, 4823–4873, <https://doi.org/10.5194/gmd-12-4823-2019>, 2019.
- Tatebe, H., Ogura, T., Nitta, T., Komuro, Y., Ogochi, K., Takemura, T., Sudo, K., Sekiguchi, M., Abe, M., Saito, F., Chikira, M., Watanabe, S., Mori, M., Hirota, N., Kawatani, Y., Mochizuki, T., Yoshimura, K., Takata, K., O’Ishi, R., Yamazaki, D., Suzuki, T., Kurogi, M., Kataoka, T., Watanabe, M., and Kimoto, M.: Description and basic evaluation of simulated mean state, internal variability, and climate sensitivity in MIROC6, *Geoscientific Model Development*, 12, 2727–2765, <https://doi.org/10.5194/gmd-12-2727-2019>, 2019.
- 595 Tebaldi, C. and Knutti, R.: The use of the multi-model ensemble in probabilistic climate projections, *Philosophical Transactions of the Royal Society A: Mathematical, Physical and Engineering Sciences*, 365, 2053–2075, <https://doi.org/10.1098/rsta.2007.2076>, <http://rsta.royalsocietypublishing.org/cgi/doi/10.1098/rsta.2007.2076>, 2007.
- 600 Tokarska, K. B., Stolpe, M. B., Sippel, S., Fischer, E. M., Smith, C. J., Lehner, F., and Knutti, R.: Past warming trend constrains future warming in CMIP6 models, *Science Advances*, 6, eaaz9549, <https://doi.org/10.1126/sciadv.aaz9549>, <https://advances.sciencemag.org/lookup/doi/10.1126/sciadv.aaz9549>, 2020.
- van Vuuren, D. P., Edmonds, J., Kainuma, M., Riahi, K., Thomson, A., Hibbard, K., Hurtt, G. C., Kram, T., Krey, V., Lamarque, J. F., Masui, T., Meinshausen, M., Nakicenovic, N., Smith, S. J., and Rose, S. K.: The representative concentration pathways: An overview, *Climatic Change*, 109, 5–31, <https://doi.org/10.1007/s10584-011-0148-z>, 2011.
- 605 Voldoire, A., Saint-Martin, D., Sénési, S., Decharme, B., Alias, A., Chevallier, M., Colin, J., Guérémy, J., Michou, M., Moine, M., Nabat, P., Roehrig, R., Salas y Méliá, D., Séférian, R., Valcke, S., Beau, I., Belamari, S., Berthet, S., Cassou, C., Cattiaux, J., Deshayes, J., Douville, H., Ethé, C., Franchistéguy, L., Geoffroy, O., Lévy, C., Madec, G., Meurdesoif, Y., Msadek, R., Ribes, A., Sanchez-Gomez, E., Terray, L., and Waldman, R.: Evaluation of CMIP6 DECK Experiments With CNRM-CM6-1, *Journal of Advances in Modeling Earth Systems*, 11, 2177–2213, <https://doi.org/10.1029/2019MS001683>, <https://onlinelibrary.wiley.com/doi/abs/10.1029/2019MS001683>, 2019.
- 610 Yang, Y.-M., Wang, B., Cao, J., Ma, L., and Li, J.: Improved historical simulation by enhancing moist physical parameterizations in the climate system model NESM3.0, *Climate Dynamics*, 54, 3819–3840, <https://doi.org/10.1007/s00382-020-05209-2>, <https://doi.org/10.1007/s00382-020-05209-2>, 2020.
- 615 Yukimoto, S., Kawai, H., Koshiro, T., Oshima, N., Yoshida, K., Urakawa, S., Tsujino, H., Deushi, M., Tanaka, T., Hosaka, M., Yabu, S., Yoshimura, H., Shindo, E., Mizuta, R., Obata, A., Adachi, Y., and Ishii, M.: The meteorological research institute Earth system model version 2.0, MRI-ESM2.0: Description and basic evaluation of the physical component, *Journal of the Meteorological Society of Japan*, 97, 931–965, <https://doi.org/10.2151/jmsj.2019-051>, 2019.
- 620 Zelinka, M. D., Myers, T. A., McCoy, D. T., Po-Chedley, S., Caldwell, P. M., Ceppi, P., Klein, S. A., and Taylor, K. E.: Causes of Higher Climate Sensitivity in CMIP6 Models, *Geophysical Research Letters*, 47, 1–12, <https://doi.org/10.1029/2019GL085782>, <https://onlinelibrary.wiley.com/doi/abs/10.1029/2019GL085782>, 2020.